Intracellular accumulation and immunological response of NIR-II polymeric nanoparticles

Iryna Moskalevska, Virginie Faure, Lucie Haye, Marion Mercey-Ressejac, Arindam Dey, Benoit Chovelon, Lohona Soro, Loïc Charbonnière, Andreas Reisch, Andrey Klymchenko, et al.

Intracellular accumulation and immunological response of NIR-II polymeric nanoparticles

Iryna Moskalevska[1], Virginie Faure[1], Lucie Haye[2], Marion Mercey-Ressejac[3,4], Arindam K. Dey[3], Benoit Chovelon[5], Kevin Soro[6], Loïc J. Charbonnière[6], Andreas Reisch[2], Andrey S. Klymchenko[2], Patrice N. Marche[3], Jean-Luc Coll[1], Zuzana Macek Jilkova[3,4], Xavier le Guével[1*]

[1] Cancer Targets & Experimental Therapeutics, Institute for Advanced Biosciences (IAB), University of Grenoble Alpes (UGA)/ INSERM-U1209 / CNRS-UMR 5309- Grenoble, France
[2] Université de Strasbourg, CNRS, Laboratoire de Bioimagerie et Pathologies UMR 7021, Strasbourg F-67000, France
[3] Institute for Advanced Biosciences (IAB), University of Grenoble Alpes (UGA)/ INSERM-U1209 / CNRS-UMR 5309- Grenoble, France
[4] Service d'hépato-gastroentérologie, Pôle Digidune, CHU Grenoble Alpes, 38700 La Tronche, France
[5] Institut de Biologie et Pathologie, CHU de Grenoble-Alpes, France
[6] Equipe de Synthèse Pour l'Analyse (SynPA), Institut Pluridisciplinaire Hubert Curien (IPHC), UMR 7178, CNRS, Université de Strasbourg, ECPM, 25 rue Becquerel, 67087, Strasbourg Cedex, France.

ABSTRACT

The innate immune system presents the first line of host defence. When designing new nanomedicine probes, it is therefore crucial to understand how these probes interact with it. We prepared highly monodisperse, well defined, and stable polymeric nanoparticles (NPs) loaded with gold nanoclusters (Au NCs) which provide fluorescence emission in the NIR-II (900-1700 nm) optical window suitable for *in vivo* imaging. Au NCs loaded in polymeric NPs are potentially of great interest as they could be used as biosensors, delivery and therapeutic agents. After their molecular characterization, their interaction with macrophages and their immunological properties were investigated in detail. The NIR-II emitting polymeric NPs showed an efficient cellular uptake to more than 70% in time and in dose-dependent manner. While the NPs did not produce any immunotoxicity, it was reported an anti-inflammatory response and a strong down-regulation of nitric oxide level after LPS stimulation.

Keyword: NIR-II; immune response; gold nanoclusters; nitric oxide

INTRODUCTION

The design of biodegradable and biocompatible polymer nanoparticles has greatly expanded the range of applications of nanomedicines in the fields of bioimaging and therapeutical applications against cancers [1]. With the capacity to tailor polymeric NPs as

swiss army knives with imaging modalities, drug delivery and targeting features, perspectives are opened to offer new theranostic agents for personalized medicine[2].
Optical modalities to monitor non-invasively theranostic agents are highly desirable and the near-infrared window between 900 and 1700 nm, called NIR-II, offers a greater detection in-depth compared to the visible and to the first infrared window (700- 900 nm)[3-6]. Various NIR-II contrast agents have been developed over the past few years made of organic dyes (cyanines, BODIPY)[7, 8], inorganic fluorophores (SWCNs, Lanthanides)[9, 10] or nanocrystals (Quantum Dots)[11, 12], each of them presenting their advantages and their drawbacks in terms of brightness, biocompatibility and photostability[13]. Gold nanoclusters (Au NCs) are an interesting class of NIR-II emitters with an ultra-small size below 3 nm. Their NIR-II photoluminescence (PL) is tunable by controlling their number of atoms and their surface chemistry[14-18]. Furthermore, the ability to functionalise their surface is favourable for high loading in numerous nanocarriers[19, 20] as well as encapsulation into biomolecules such as proteins[21-23].
Polymeric NPs are highly suitable nanosystems to act both as delivery system and carry high numbers of fluorescent emitters[24, 25]. Based on the high versatility to tailor size, surface charge and loading of polymeric NPs, we designed monodisperse poly(ethyl methacrylate (PEMA) NPs loaded with hydrophobic photoluminescent Au NCs.[26, 27]. Because the first line of cells in contact in the body are innate immune cells such as macrophages, we investigated the interaction and the intracellular accumulation of these NIR-II emitting PEMA NPs with macrophages. We also evaluated the capacity of PEMA NPs to modulate immunological responses of macrophages with or without stimulation with lipopolysaccharide (LPS).

EXPERIMENTAL SECTION

All chemical products were purchased from Sigma-Aldrich (France). PEMA bearing 5 mol% of methacrylic acid was synthetized through free radical polymerization as described previously [27, 28].

Synthesis and characterisations of particles. Gold nanoclusters stabilized by dodecanethiol (DDT) called here **AuDDT** were prepared as described elsewhere[29]. Briefly, 46.4 mg (93.75 μmol) $AuClPPh_3$ was dispersed in ethanol with the addition of 81.5 mg (0.94 μmol) *tert*-butylamine-borane for 45 min with fast stirring. The colour of the solution changed from orange-red to black after 5 min. Then 12 μL of DDT were added and the mixture was left to stir for another 3 hours. The dark solution was then filtered 3 times with filters at 3kDa cut-off to remove unreactive species and kept refrigerated.
Preparation of NPs: Stock solutions of PEMA were prepared at a concentration of 10 $g.L^{-1}$ in acetonitrile. These solutions were diluted to 2 $g.L^{-1}$ in acetonitrile, with or without 10 wt% of AuDDT (relative to the polymer). These solutions were quickly added to a 9-fold volume excess of phosphate buffer (20 mM, pH 7.4) under shaking (Thermomixer comfort, Eppendorf, 1050 rpm at 21°C), followed by further dilution to the desired concentration. A similar procedure was used to load the dye salt R18/F5-TPB (rhodamine B octadecyl ester with tetrakis(pentafluorophenyl)borate as counterion) in PEMA NPs of the same particle size, as previously described[30].
Dynamic light scattering (DLS) and ζ-potential: The size and ζ-potential of the mixed polymer NPs were measured on a Zetasizer Nano series ZSP (Malvern Instruments S.A.). For size determination, each sample was measured 10 times with a run length of 10 s each. The volume average values, determined by the Zetasizer software (Malvern) based on Mie theory,

were used. Mean values give the average over at least three independent preparations, error bars correspond to standard error of the mean. For ζ-potential determination three successive measurements combining electrophoretic mobility and laser Doppler velocimetry with > 10 runs each were carried out with an applied potential of ±150 V.

Transmission electron microscopy (TEM): Solutions of NPs (5 µL) were deposited onto carbon-coated copper−rhodium electron microscopy grids following air or amylamine glow-discharge. They were then treated for 20 s with a 2% uranyl acetate solution for staining. The obtained grids were observed using a Tecnai F20 Twin transmission electron microscope (FEI Eindhoven Holland) operating at a voltage of 200 kV. Images (2,048 pixels × 2,048 pixels) were recorded using a US1000 camera (Gatan) and analyzed using the Fiji software. At least 200 particles per condition were analyzed.

Spectroscopic properties: Absorption spectra were recorded on a Cary 4000 Scan ultraviolet−visible spectrophotometer (Varian). Emission spectra were performed with 10 × 10 mm² quartz suprasil certified cells (Helma Analytics). The steady state emission spectra were recorded on an Edinburgh Instrument FLP920 spectrometer working with a continuous 450-W Xe Lamp and a Hamamatsu R5 509-72 photomultiplier for NIR detection. Then, 850-nm high-pass filter was used to eliminate the second-order artefacts when recording the NIR spectra. Excitation was performed at 415nm.

Gold loading in polymeric NPs was determined using a quadrupole Inductively coupled plasma mass spectrometry (ICP-MS) (Perkin Elmer NexION 2000, Waltham, MA, USA). Standard solutions were prepared in aqua regia 3% (v/v). ^{197}Au was measured using ^{103}Rh at 141 nmol/L was used as internal standard.

Cell culture. Both the J774.1A murine macrophage cell line (ATCC) and the NIH-3T3 murine embryonic fibroblast cell line (ATCC) were cultured in DMEM supplemented with 10% foetal calf serum at 37°C, 5% CO_2.

Cytotoxicity. Cytotoxicity was assessed by two different methods: PrestoBlueTM and lactic dehydrogenase (LDH) release assays. Cells were seeded in 96 well-plates at 3000 cells/well for J774.1A and 5000 cells/well for 3T3. After 24 h, cells were treated with different concentrations of nanoparticles (5, 10, 25, 50 and 100 µg/mL for PEMA NPs) for 24 or 48 h. PrestoBlueTM (Thermofisher cat n° A13261) was added at 1:10 and incubated for 3h. The absorbance was read at 570 nm using a 595 nm reference with the SunriseTM reader (Tecan). The released LDH from cells with damaged membranes was quantified using the CytoTox-ONE assay kit according to the manufacturer's protocol (Promega cat n° G7891). The fluorescence signal was read at 560 nm for an excitation at 590 nm with CLARIOstar® Microplate Reader (BMG Labtech).

Cellular uptake. The cellular interaction kinetics of loaded PEMA NPs were assessed by flow cytometry using R18/F15-TPB loaded PEMA NPs. J774.1A were seeded at 10^5 cells/mL and, after 24h, incubated for different periods from 0 to 24h and 0 to 100 µg/mL R18/F15TPB-PEMA NPs concentrations. The cells were fixed with paraformaldehyde 4% and the cellular interaction was assessed using BDTM LSR II (BD Biosciences). The fluorescence of R18/F15TPB -PEMA NPs was detected using the band pass 525/50 upon a 488 nm excitation.

The cellular uptake of Au-PEMA NPs was validated by confocal microscopy. J774.1A were first seeded at $5x10^4$ cells/mL on coverslips and then incubated with Au-PEMA NPs (50µg/mL) for 24 h at 37°C. Cells were fixed in paraformaldehyde 4% and permeabilized by Triton 0.2% BSA 4%. They were then labelled with Alexa FluorTM 488 Phalloidin (Thermofisher cat n°: A12379).

The intracellular fate of the nanocarriers was studied by live-cell confocal microscopy. J774.1A cells were seeded at $5x10^4$ cells/mL in 4-well LabTeck and after 24h incubated with Au-PEMA NPs (50 µg/mL) for 24 h. The cells were labelled with Cell mask green plasma membrane™ (Thermofisher cat n°: C37608). All confocal measurents were done using an LSM710 NLO confocal microscope (Carl Zeiss) with an objective Plan Apochromat 20×/0.8 NA in air and an objective Plan Apochromat 63×/1.4 NA in oil. Near-infrared signal from Au NCs was captured using APD detector with a 405 nm excitation and a LP750 filter. Image treatment was done using the ImageJ software.
The gold uptake quantification was determined by ICP-MS. Cells were mineralized at atmospheric pressure in aqua regia (nitric acid and hydrochloric acid in a molar ratio of 1:3), for 48 h at room temperature. The mineralization is diluted to reach a concentration of 3% of aqua regia before analysis. Standard solutions were prepared in aqua regia 3% (v/v).

Immunotoxicity. J774.1A were seeded at $2.5x10^5$ cells/mL. After 2 h, the cells were treated with different concentrations of nanocarriers (10 and 50 µg/mL) for 24h. The nanocarrier exposed cells were stimulated with *E. coli* lipopolysaccharide (LPS) at 2 µg/mL for 24 h at 37°C, 5% CO_2.
Macrophages were identified by the expression of markers CD11b (BioLegend cat n°: 101226) and F4/80 (BioLegend cat n°: 123152), and their activation was evaluated by the expression of $I\text{-}A^b$ (BioLegend cat n°: 116410) and CD86 (BioLegend cat n°: 105008). Live cells were selected by Zombie VioletTM staining (BioLegend cat n°: 423113). Fluorescence labelled cells were analysed by flow cytometry using LSR II (BD Biosciences) using FCS Express V6 software (De Novo Software).
Cytokines production was measured in the supernatant of cell cultures using IL-6, TNF-α, and IL-10 mouse ELISA kits following the manufacturer's protocols (Thermofisher cat n°: 887064, 88732488, 88710588). The absorbance was read with CLARIOstar® Microplate Reader (BMG Labtech) at 450 nm using 570 nm as a reference.
The NO production was evaluated by measuring the nitrite concentration in the cell culture supernatant using Griess assay. 50 µL of supernatant was incubated with the same volume of Sulphanilamide 1% (w/v) (Sigma cat n°: S9251) for 10 min under shaking at 37°C. 50 µL of N-alpha-naphthyl-ethylenediamine (NED) 0.1% (w/v) (Sigma cat n°: 222488) was added and incubated for 10 min at 37°C in the dark. The absorbance was read with CLARIOstar® Microplate Reader (BMG Labtech) at 540 nm.
Production of ROS in the cell culture supernatant was estimated following the manufacturer's protocol (ENZO ROS/superoxide detection kit ref: ENZ-51010).

Statistical analysis. The values are presented by mean ± standard error of mean (SEM). At least three independent experiments were performed. Data were tested for normality and the appropriate statistic test was chosen. The statistical analysis was performed by Kruskal-Wallis test for multiple means comparisons of non-parametric data using GraphPad Prism software version 8.0. The probability was set at *p-value < 0.05, **p-value < 0.01, ***p-value < 0.001.

RESULTS & DISCUSSION

1- Characterisation of NIR-II polymeric NPs

AuDDT prepared by wet chemistry (see experimental detail, **Fig.S1A**) possessed a core size smaller than 2.5 nm as confirmed by HRTEM (**Fig. S1B**). Unlike others Au NCs, AuDDT showed in solution multiple absorption bands at 390 nm, 420 nm, 450 nm, 545nm, 700 nm, 750 nm (**Fig. S1C**). To note that the absorption bands at 390 nm, 450 nm and ~670 nm and the shoulder at 800 nm are usually attributed to the molecular species $Au_{25}SR_{18}$[31] (SR= DDT in our case) which suggested a high population of $Au_{25}DDT_{18}$ within the AuDDT sample. AuDDT showed a good stability in ethanol, chloroform, and acetonitrile during a few weeks at room temperature enabling their loading in the polymer PEMA.

The AuDDT NCs were then encapsulated into PEMA polymer NPs through nanoprecipitation (**Fig. 1A**) at a loading of 10 wt% relative to the polymer (Au-PEMA).

The loading was confirmed by ICP-MS measurement. DLS measurements in water indicated an hydrodynamic diameter of Au-PEMA NPs around 33±3 nm (**Fig. 1A**) in agreement with the size measured by TEM at 26±5 nm (**Fig. 1B, C**). Both, the polydispersity index from DLS (0.20) and size distribution observed in TEM, indicated a monomodal population with low polydispersity. The surface charge determined by zeta potential confirmed also their negative charge (-31 mV) in water at pH 7, in line with the observed good colloidal stability over several months (at 4°C).

Loading AuDDT in a polymeric matrix did not affect their absorbance properties as shown by a similar absorption profile for AuDDT in acetonitrile and loaded in PEMA NPs as illustrated in **Fig. 1D**. Direct dispersion of AuDDT in water (without polymer) led to cloudy samples with a broad absorbance spectrum, indicating strong scattering and aggregation of the NCs **(Fig. 1D)**. The fact that this behaviour was not observed when using AuDDT with the polymer supported the efficient entrapment of AuDDT in the polymer NPs.

Au NCs have shown recently high interest as NIR-II emitters due to their broad absorption in the visible and the red/near-infrared region (600-900 nm) and their relatively intense NIR-II emission that could be tuned by controlling their core size and surface chemistry[5, 6, 14, 16, 17, 32]. AuDDT showed broad NIR-II photoluminescence (PL) emission typical of Au NCs with a shoulder at 950 nm, a maximum peak at 1050 nm and a second shoulder at 1200 nm which have been assigned to interdependent energy transfer taking place with the gold core and at the surface of the core (**Fig.1E**)[17, 18, 33]. The fluorescence emission of Au-PEMA NPs seems not sensitive to the excitation wavelength with the same profile at 405 nm and 730 nm excitation (**Fig. S1D**). Compared to free AuDDT in acetonitrile, PL of Au-PEMA NPs has higher intensity (2.3-fold) with broader emission among the longer wavelength. We confirmed again the poor stability of free AuDDT in water which led to the fall of the PL as depicted in **Fig. 1E**.

We did not notice any PL decrease over a period of a few weeks nor photobleaching during the cellular studies that demonstrated the robustness of this protocol to load hydrophobic Au NCs such as AuDDT inside these ~30 nm polymeric PEMA NPs.

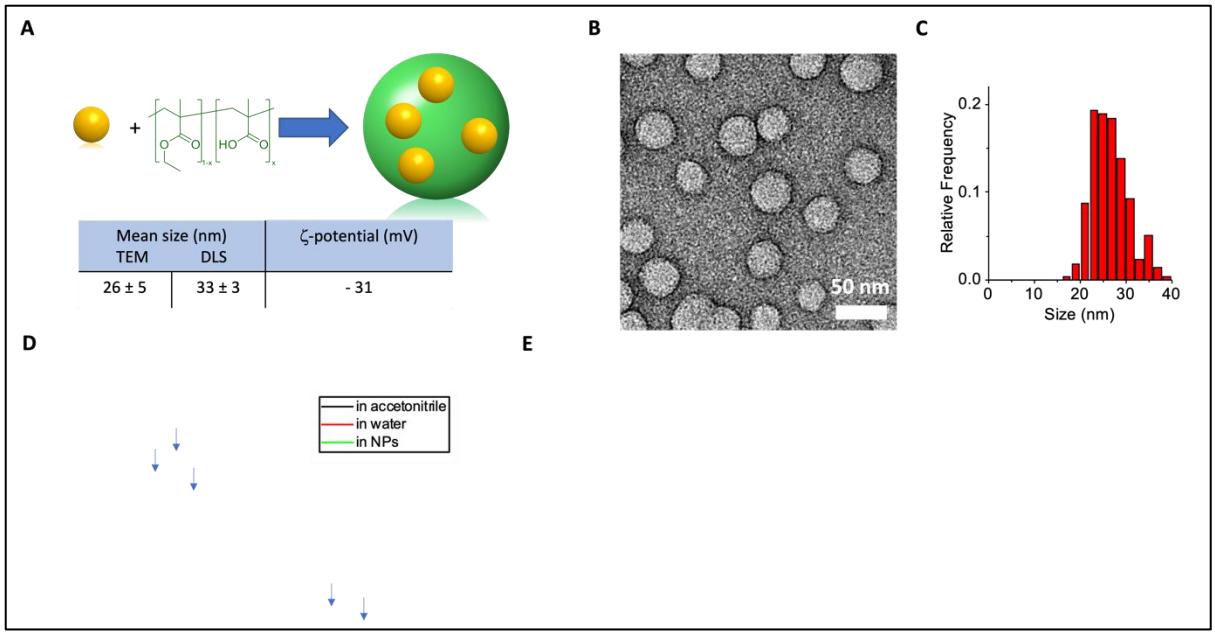

Figure 1. NP characterization. A) Scheme of AuDDT loading in PEMA NPs. B) TEM image of Au-PEMA NPs in water and C) their corresponding particle size distribution (n_{NPs}>100). D) Absorbance and E) Fluorescence spectra of AuDDT dispersed in acetonitrile, in water, and Au-PEMA in water ($\lambda_{exc.}$ 415 nm).

2- Cytotoxicity and cellular uptake

Cell viability of J774.1A macrophages in presence of Au-PEMA NPs was evaluated by presto-blue assays after 24h and 48h incubation using particle concentrations between 1 to 100 μg/mL. No cytotoxicity was observed in such conditions (**Fig. 2A**) using also LDH assays and with another cell lines such as mouse embryonic fibroblast (**Fig. S2**). This enabled us to move forward to study the cellular uptake of Au-PEMA NPs in macrophages as a function of the particle concentration and the incubation time.

Cellular interaction of 30 nm fluorescent PEMA NPs was assessed by flow cytometry as a function of time up to 24h at 50 μg/mL. Because the Au NC fluorescence emission is out of the range of the flow cytometry detection window, we used rhodamine dye (R18 F5-TPB) loaded PEMA NPs of similar size (22±3 nm; PDI = 0.17), which were prepared using the same protocol. However, taking into account previous works on fluorophore loaded PEMA and other polymer NPs and the particle characterization performed in Au-PEMA NPs, we assumed a similar cellular behaviour of the 30 nm PEMA NPs independently of the loading.[24, 28, 34]

There was a clear increase, over the time of exposure, of the quantity of fluorescence associated with macrophages and of the number of macrophages associated with PEMA NPs, reaching 69.8% after 24h as seen in **Fig. 2B and S3**.

In order to confirm this result, we quantified the amount of gold from Au-PEMA in macrophages using the same experimental conditions by ICP-MS. Results indicated an increase in the gold content in cells with time and with the particle concentration (**Fig. 2C**).

In another series of experiments, we looked at the influence of the particle concentration on the cellular interaction. Flow cytometry experiment (**Fig. 2D, S3**) performed at 24h using a wide range of fluorescent PEMA particle concentrations from 0 to 100 μg/mL showed a constant increase of the cellular interaction up to 76% which also agreed with the trend observed by ICP-MS at two different particle concentrations (10 and 50 μg/mL).

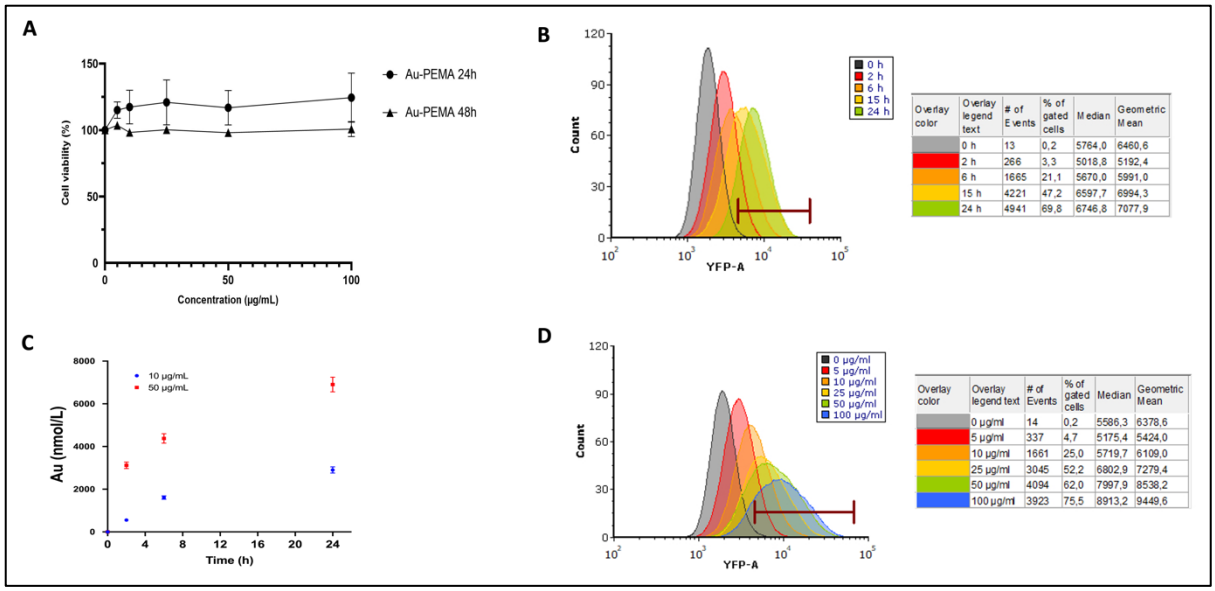

Overlay color	Overlay legend text	# of Events	% of gated cells	Median	Geometric Mean
	0 h	13	0,2	5764,0	6460,6
	2 h	266	3,3	5018,8	5192,4
	6 h	1665	21,1	5670,0	5991,0
	15 h	4221	47,2	6597,7	6994,3
	24 h	4941	69,8	6746,8	7077,9

Overlay color	Overlay legend text	# of Events	% of gated cells	Median	Geometric Mean
	0 µg/ml	14	0,2	5586,3	6378,6
	5 µg/ml	337	4,7	5175,4	5424,0
	10 µg/ml	1661	25,0	5719,7	6109,0
	25 µg/ml	3045	52,2	6802,9	7279,4
	50 µg/ml	4094	62,0	7997,9	8538,2
	100 µg/ml	3923	75,5	8913,2	9449,6

Figure 2. Flow cytometry. A) Evaluation of Au-PEMA toxicity on J774.1A macrophages. Cell viability was analyzed by PrestoBlue after 24h and 48h incubation with Au-PEMA NPs. Mean ± SE, n = 3. B) Uptake of NP loaded with R18 F5-TPB as a function of time at 50 µg/mL, using the YFP filter. C) ICP-MS measurements to determine the gold content in J774.1A macrophages incubated with Au-PEMA at different concentrations and incubation times. D) Uptake of NP loaded with R18 F5-TPB as a function of concentration after 24h of incubation, using the YFP filter.

In order to determine whether Au-PEMA NPs accumulated on the membrane or inside the cells, we conducted confocal fluorescence microscopy. We could track the Au-PEMA NPs thanks to a highly sensitive APD camera enabling to detect fluorescence signal up to 1000 nm suitable for the NIR-II emission of the Au NC emitters. In **Fig. 3A**, the accumulation of AuPEMA NPs (in red) in the cytoplasm was clearly observed after 24 h incubation at 50 µg/mL. Kinetic experiments conducted at short incubation times (5 min, 30 min) indicated a fast interaction of the NPs with the cellular membrane after 5 min, followed by their internalization as seen at 30 min (**Fig. 3B**). This particle uptake is commonly associated with an endocytic process where particles are first interacting with the cell membrane and then are engulfed into endosomes vesicles until their late storage in lysosomes[35].

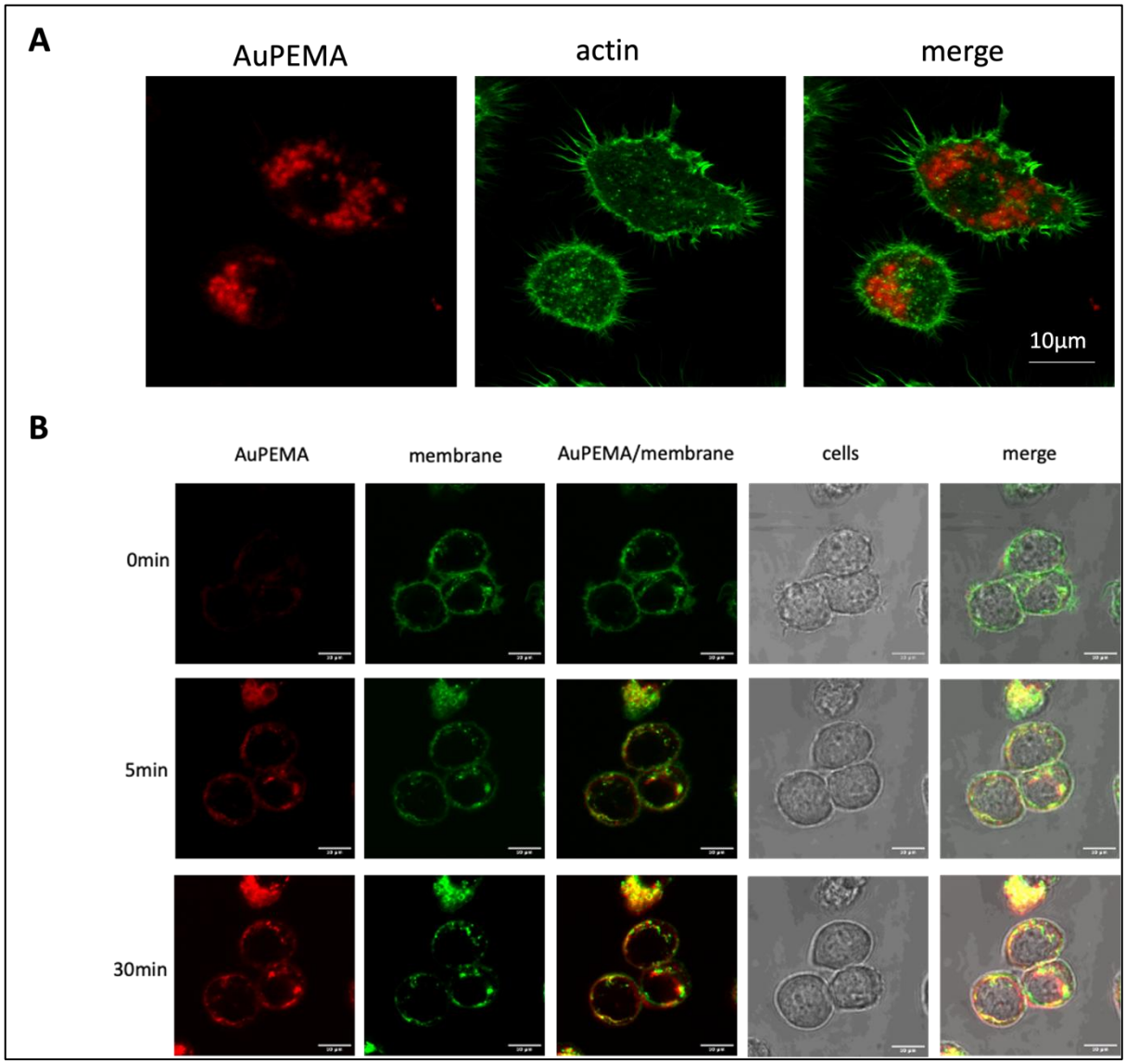

Figure 3. Confocal microscopy. A) CLSM of J774.1A macrophages were incubated with Au-PEMA (red) at 50µg/mL for 24h and labelled for actin (in green). B) Measurements performed at t = 0, 5min, 30 min after incubating Au-PEMA (50µ/mL in DMEM with 10% FBS; in red) with J774.1A cells (membrane in green).

3- Immunological response

We then investigated the immunological response of J774.1A macrophages in presence of Au-PEMA NPs (30±3 nm) or with the unloaded PEMA NPs (27±1 nm) by first looking at their activation and their cytokine secretion. We observed a slight activation of the macrophages in presence of the unloaded PEMA NPs at high concentration (50 µg/mL) from 60% to 90% while no significant effect is detected using the loaded Au-PEMA NPs as seen in **Fig. 4A**. In the second set of experiments, we intended to determine if the presence of NPs modifies the macrophage activation after a stimulation with LPS. Results presented in **Fig.4A** show no significant impact of PEMA NPs or Au-PEMA NPs at 10 and 50 µg/mL of NPs. This suggests that the polymer with or without Au NCs did not alter the activation of these macrophages at this concentration range. To determine whether these NPs elicited pro-inflammatory or an anti-inflammatory response, we then checked the levels of indicative cytokins (IL-6, TNF-α, IL-10) secreted by macrophages. Results depicted in **Fig. 4B, C, D**

show almost undetectable levels of cytokines secreted by macrophages exposed to PEMA NPs or Au-PEMA NPs. After LPS stimulation, IL-6 and TNF-α levels slightly decreased for the loaded and the unloaded NPs at the highest particle concentration when compared to LPS-stimulated cells without any NP, but these variations were not statically significant. These data suggest a moderate, if any, anti-inflammatory effect after stimulation due to the presence of the polymer PEMA and independently of the loading in our case. This anti-inflammatory effect has been reported with others polymeric NPs such as PLGA and PLA NPs[36, 37]. This trend was also observed for IL-10 which is associated with regulatory response[38].

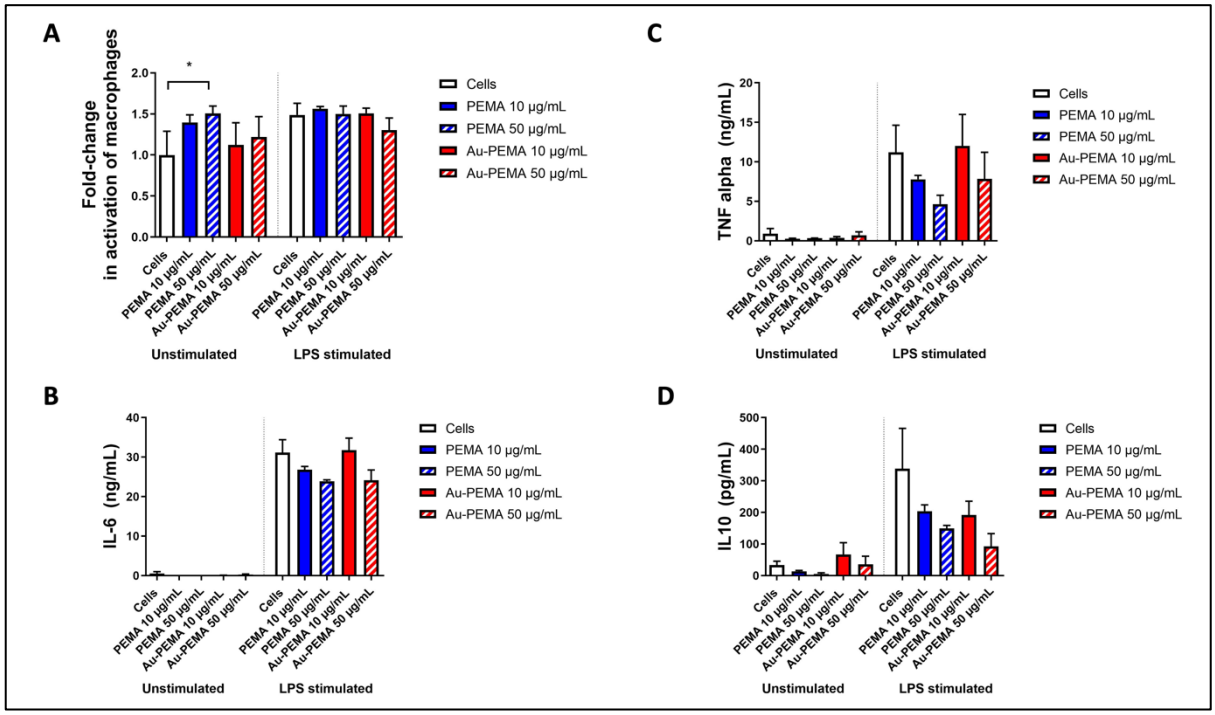

Figure 4. **Effect of the Au-PEMA on macrophage activation .** A) Percentage of activated J774.1A macrophages determined as the percentage of cells expressing the CD86 and MHCII markers after a 24h exposure to NPs, followed by a 24h of LPS stimulation. Secretion of cytokines B) IL-6, C) TNF-α and D) IL-10 by J774.1A after a 24h exposure to NPs, followed by a 24h of LPS stimulation. Mean ± SE. PEMA control groups n = 3; other groups n= 7-8.

To further seek for potential anti-inflammatory effect of the Au-PEMA, we analysed the production of reactive oxygen species (ROS) and of nitric oxide (NO), which both play an essential role in cell regulation and are associated to inflammation[39, 40].

We did not observe any detectable NO production by unstimulated macrophages, even in the presence of Au-PEMA NPs demonstrating the lack of proinflammatory potential. During the LPS-induced inflammatory response, macrophages release NO which is a key proinflammatory mediator[41]. As expected, cells stimulated with LPS produced a high NO level (30µM), **Fig. 5A**. However, we noticed a striking decrease of the NO production in presence of Au-PEMA. This trend was not affected by the Au loading of the PEMA, since we observed a similar decrease for PEMA NPs and for Au-PEMA NPs in a dose-dependent manner (Refere to new FigS). For instance, NO production decreased by 30% at 10 µg/mL of Au-PEMA and by more than 85% at 50 µg/mL of Au-PEMA. These findings corroborated the previous results suggesting the possible anti-inflammatory effect of NPs.

Next, we focused on ROS. We observed no difference in the ROS production by the unstimulated macrophages exposed to Au-PEMA (**Fig. 5B**) nor to PEMA (Refer to new FigS) compared to control cells, Contrarily to NO production after LPS stimulus, there were no significant changes of ROS production detected by our experimental aproach.

At first, we had expected a similar behaviour between the NO and the ROS level with several examples reporting the scavenging of ROS in cells by some NPs leading to a fall of NO level, as reviewed by Mauricio et al. [42]. PEMA NPs seemed then to regulate NO level by others pathways. For example, Qureshi *et al.* reported a concomitant inhibition of NO and inflammatory cytokines in LPS-stimulated murine macrophages. They hypothesized that various tested drugs, such as Resveratrol, inhibit proteasomal enzymatic activity, the production of inflammatory cytokines NO in response to LPS activation[43]. We reckon at this stage that more works are requested to fully elucidate the immuno-metabolism mechanism occurring in macrophages in the presence of PEMA NPs. The future effort may focus on *in vivo* studies to evaluate the whole-body immunological response to PEMA NPs.
Altogether these results suggest that the exposure of macrophages to PEMA NPs may decrease their inflammatory response in dose-dependent manner without compromising their activation status.

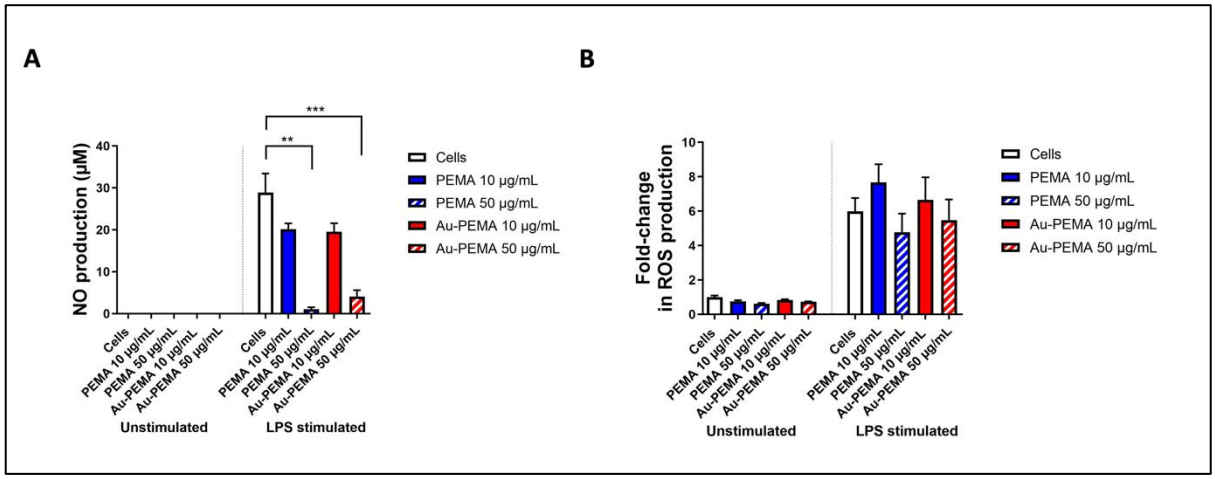

Figure 5. Effect of NP on NO and ROS production. A) NO production by J774.1A macrophages after 24h exposure to NPs, followed by a 24h of LPS stimulation. Mean ± SE. PEMA control groups n = 3; other groups n= 7-8. B) Fold-change in ROS production by J774.1A macrophages after 24h exposure to NPs, followed by a 24h of LPS stimulation. Data are normalized to unstimulated cells. Mean ± SE, n = 5.

CONCLUSION

We reported here the simple design of NIR-II emitting polymeric NPs that were efficiently taken up by murine macrophages using endocytic processes in a time and dose dependant manner. We found that the nature of the polymer matrices made of polyethylmethacrylate can lead to an anti-inflammatory effect accompanied by a down regulation of NO level after LPS stimulation. These interesting results suggest a potential use of such nanocarriers for immunoregulatory applications with the possibility to track these nanosystems non-invasively in small animals by NIR-II imaging.

Acknowledgements
XLG would like to thank ligue contre le cancer (R21004CC) for their financial support. XLG, AR, LH, KS, LJC thanks ANR LAPIN (ANR-20-CE09-0021-04)) for their financial

support. The authors also acknowledge the support and the use of resources of the French Infrastructure for Integrated Structural Biology FRISBI ANR-10-INBS-05 and of Instruct-ERIC and especially C. Crucifix for help with electron microscopy.

REFERENCES

1. Aghebati-Maleki, A., et al., *Nanoparticles and cancer therapy: Perspectives for application of nanoparticles in the treatment of cancers.* Journal of Cellular Physiology, 2020. **235**(3): p. 1962-1972.
2. Johnson, K.K., et al., *Preclinical Cancer Theranostics—From Nanomaterials to Clinic: The Missing Link.* Advanced Functional Materials, 2021. **31**(43): p. 2104199.
3. Liu, P., et al., *The Near-Infrared-II Fluorophores and Advanced Microscopy Technologies Development and Application in Bioimaging.* Bioconjugate Chemistry, 2020. **31**(2): p. 260-275.
4. Zhu, S., et al., *Near-Infrared-II Molecular Dyes for Cancer Imaging and Surgery.* Advanced Materials, 2019. **31**(24): p. 1900321.
5. Musnier, B., et al., *Optimization of spatial resolution and scattering effects for biomedical fluorescence imaging by using sub-regions of the shortwave infrared spectrum.* Journal of Biophotonics, 2020. **n/a**(n/a): p. e202000345.
6. Kong, Y., et al., *A NIR-II-emitting gold nanocluster-based drug delivery system for smartphone-triggered photodynamic theranostics with rapid body clearance.* Materials Today, 2021. **51**: p. 96-107.
7. Godard, A., et al., *Water-Soluble Aza-BODIPYs: Biocompatible Organic Dyes for High Contrast In Vivo NIR-II Imaging.* Bioconjugate Chemistry, 2020. **31**(4): p. 1088-1092.
8. Carr, J.A., et al., *Shortwave infrared fluorescence imaging with the clinically approved near-infrared dye indocyanine green.* Proceedings of the National Academy of Sciences, 2018. **115**(17): p. 4465.
9. Yang, Y., et al., *Recent advances in design of lanthanide-containing NIR-II luminescent nanoprobes.* iScience, 2021. **24**(2): p. 102062.
10. Hong, G., et al., *Through-skull fluorescence imaging of the brain in a new near-infrared window.* Nature Photonics, 2014. **8**(9): p. 723-730.
11. Bruns, O.T., et al., *Next-generation in vivo optical imaging with short-wave infrared quantum dots.* Nature Biomedical Engineering, 2017. **1**(4): p. 0056.
12. Zebibula, A., et al., *Ultrastable and Biocompatible NIR-II Quantum Dots for Functional Bioimaging.* Advanced Functional Materials, 2018. **28**(9): p. 1703451.
13. Li, J., et al., *Recent advances in the development of NIR-II organic emitters for biomedicine.* Coordination Chemistry Reviews, 2020. **415**: p. 213318.
14. Chen, Y., et al., *Shortwave Infrared in Vivo Imaging with Gold Nanoclusters.* Nanoletters, 2017. **17**(10): p. 6330-6334.
15. Musnier, B., et al., *High photoluminescence of shortwave infrared-emitting anisotropic surface charged gold nanoclusters.* Nanoscale, 2019. **11**(25): p. 12092-12096.
16. Yu, Z., et al., *High-Resolution Shortwave Infrared Imaging of Vascular Disorders Using Gold Nanoclusters.* ACS Nano, 2020. **14**(4): p. 4973-4981.
17. Liu, H., et al., *Atomic-Precision Gold Clusters for NIR-II Imaging.* Advanced Materials, 2019. **31**(46): p. 1901015.
18. Le Guével, X., et al., *Tailoring the SWIR emission of gold nanoclusters by surface ligand rigidification and their application in 3D bioimaging.* Chemical Communications, 2022.

19. Le Guével, X., et al., *NIR-emitting fluorescent gold nanoclusters doped in silica nanoparticles.* Journal of Materials Chemistry, 2011. **21**(9): p. 2974-2981.
20. Tseng, W.-B., et al., *Synthesis of gold nanoclusters-loaded lysozyme nanoparticles for ratiometric fluorescent detection of cyanide in tap water, cyanogenic glycoside-containing plants, and soils.* Environmental Research, 2021: p. 112144.
21. Wang, W., et al., *Engineering the Protein Corona Structure on Gold Nanoclusters Enables Red-Shifted Emissions in the Second Near-infrared Window for Gastrointestinal Imaging.* Angewandte Chemie International Edition, 2020. **59**(50): p. 22431-22435.
22. Franck, B., et al., Research Square, 2022.
23. Xie, J., Y. Zheng, and J.Y. Ying, *Protein-Directed Synthesis of Highly Fluorescent Gold Nanoclusters.* Journal of the American Chemical Society, 2009. **131**(3): p. 888-889.
24. Reisch, A. and A.S. Klymchenko, *Fluorescent Polymer Nanoparticles Based on Dyes: Seeking Brighter Tools for Bioimaging.* Small, 2016. **12**(15): p. 1968-1992.
25. Shi, J., et al., *Cancer nanomedicine: progress, challenges and opportunities.* Nature Reviews Cancer, 2017. **17**(1): p. 20-37.
26. Reisch, A., et al., *Tailoring Fluorescence Brightness and Switching of Nanoparticles through Dye Organization in the Polymer Matrix.* ACS Applied Materials & Interfaces, 2017. **9**(49): p. 43030-43042.
27. Rosiuk, V., et al., *Controlling Size and Fluorescence of Dye-Loaded Polymer Nanoparticles through Polymer Design.* Langmuir, 2019. **35**(21): p. 7009-7017.
28. Combes, A., et al., *Protein-like particles through nanoprecipitation of mixtures of polymers of opposite charge.* Journal of Colloid and Interface Science, 2022. **607**: p. 1786-1795.
29. Li, Y., et al., *Controllable synthesis of gold nanoparticles with ultrasmall size and high monodispersity via continuous supplement of precursor.* Dalton Transactions, 2012. **41**(38): p. 11725-11730.
30. Reisch, A., et al., *Collective fluorescence switching of counterion-assembled dyes in polymer nanoparticles.* Nature Communications, 2014. **5**(1): p. 4089.
31. Jin, R., et al., *Atomically Precise Colloidal Metal Nanoclusters and Nanoparticles: Fundamentals and Opportunities.* Chemical Reviews, 2016. **116**(18): p. 10346-10413.
32. Li, D., et al., *Gold Nanoclusters for NIR-II Fluorescence Imaging of Bones.* Small, 2020. **16**(43): p. 2003851.
33. Zhou, M. and Y. Song, *Origins of Visible and Near-Infrared Emissions in [Au25(SR)18]− Nanoclusters.* The Journal of Physical Chemistry Letters, 2021. **12**(5): p. 1514-1519.
34. Andreiuk, B., et al., *Fluorescent Polymer Nanoparticles for Cell Barcoding In Vitro and In Vivo.* Small, 2017. **13**(38): p. 1701582.
35. Kettler, K., et al., *Cellular uptake of nanoparticles as determined by particle properties, experimental conditions, and cell type.* Environmental Toxicology and Chemistry, 2014. **33**(3): p. 481-492.
36. Hao, J., et al., *Neutrophils, as "Trojan horses", participate in the delivery of therapeutical PLGA nanoparticles into a tumor based on the chemotactic effect.* Drug Delivery, 2020. **27**(1): p. 1-14.
37. Saito, E., et al., *Designing drug-free biodegradable nanoparticles to modulate inflammatory monocytes and neutrophils for ameliorating inflammation.* Journal of Controlled Release, 2019. **300**: p. 185-196.

38. Iyer, S.S. and G. Cheng, *Role of interleukin 10 transcriptional regulation in inflammation and autoimmune disease.* Critical reviews in immunology, 2012. **32**(1): p. 23-63.
39. Zhao, J., *Interplay among nitric oxide and reactive oxygen species: a complex network determining cell survival or death.* Plant signaling & behavior, 2007. **2**(6): p. 544-547.
40. Sadhu, A., et al., *Nitric oxide and ROS mediate autophagy and regulate Alternaria alternata toxin-induced cell death in tobacco BY-2 cells.* Scientific Reports, 2019. **9**(1): p. 8973.
41. Chi, D.S., et al., *Regulation of nitric oxide production from macrophages by lipopolysaccharide and catecholamines.* Nitric Oxide, 2003. **8**(2): p. 127-132.
42. Mauricio, M.D., et al., *Nanoparticles in Medicine: A Focus on Vascular Oxidative Stress.* Oxidative medicine and cellular longevity, 2018. **2018**: p. 6231482-6231482.
43. Qureshi, A.A., et al., *Inhibition of nitric oxide and inflammatory cytokines in LPS-stimulated murine macrophages by resveratrol, a potent proteasome inhibitor.* Lipids in Health and Disease, 2012. **11**(1): p. 76.